

Regulation of mixotrophy in *Synechocystis* by a rhomboid protease

Iskander M. Ibrahim¹, Dale Harrison², Modesta Blunskyte-Hendley³, Bill T. Ferrara² and Elinor P. Thompson^{2,*}

Abstract

The intramembrane 'rhomboid' protease family is almost ubiquitous across evolution, with its well-conserved transmembrane domains typified in crystal structures of bacterial representatives, such as the *Escherichia coli* GlpG. In contrast with accumulating data on rhomboid function in higher organisms, where roles in human disease are an incentive for study, findings remain sparse about the functions and substrates of the prokaryotic enzymes, even though these provided the earliest protein structures. In particular, nothing at all is known about the rhomboid proteases of photosynthetic prokaryotes despite the importance of cyanobacteria as relatives of the progenitor of chloroplasts. Findings relating to the cyanobacterial enzymes would complement data on plant plastid rhomboids from work in *Arabidopsis thaliana*. *Synechocystis* sp. PCC 6803 was used, therefore, to investigate conserved photosynthetic functions across evolution for this protein family. Reverse-genetics studies using Slr1461, the single rhomboid protease of *Synechocystis* 6803, did not reveal a non-photochemical quenching phenotype as observed for the *Arabidopsis* RBL10 null mutant, which lacked a chloroplast outer membrane rhomboid. The Slr1461 mutant exhibited a marginal change in pigment composition, and its growth rate was only slightly different from that of WT under optimal light intensity. The most dramatic effect of the inactivation of Slr1461 was the mutant's distinct inability to reduce photosynthetic activity under mixotrophic conditions. Concurrent phototrophy and heterotrophy in mixotrophic growth aids survival and competitiveness in phytoplankton, allowing conservation of energy by reducing the need for uptake and fixing of CO₂ when an organic carbon source is available. It was notable, therefore, that, in the absence of the Slr1461 rhomboid, the steady-state mRNA levels were reduced for a subset of genes encoding facilitators of high-affinity CO₂ import and of transcriptional regulators of the carbon-concentrating mechanism (CCM). Slr1461 activity was also linked with that of another membrane protease, the AAA protease FtsH2, which was likewise observed to act within regulatory networks for the cyanobacterial carbon uptake mechanism. Aberrant transcript levels were most evident specifically under high CO₂ conditions, when the impact of Slr1461 enzymatic activity appeared to be upstream of NdhR, a central, controlling transcription factor of the CCM.

INTRODUCTION

The membrane-located families were the most recently discovered group of proteases, and investigations of the large 'rhomboid' class quickly proved their importance across diverse cellular processes in all kingdoms of life. They are ubiquitous across evolution, rhomboid proteases being found in prokaryotic to eukaryotic microbes, as organellar members in mitochondria and plastids, and also in the metazoa [1]. Although this early paradigm has become less fixed with accumulating research, a typical rhomboid substrate is typically a single transmembrane protein located in the lipid bilayer, from which proteolysis releases an activated peptide. A well-researched example of this is *Drosophila* Rhomboid (Rho)-1, which releases epidermal growth factor (EGF) receptor for signalling [2]. Substrate and enzyme are initially localized separately, on the endoplasmic reticulum (ER) and the Golgi apparatus, respectively [3], a mechanism that prevents cleavage of the substrate, Spitz, until it is trafficked to the ER.

Accumulating evidence for a more diverse repertoire for rhomboid action was presaged by an atypical mode of action observed when an activated intermediate was found to be retained in the membrane [4] (rather than released as an activated peptide)

Received 22 August 2025; Accepted 30 January 2026; Published 26 February 2026

Author affiliations: ¹Department of Biological Sciences, University of Towson, Maryland, 21252, USA.; ²Faculty of Engineering and Science, University of Greenwich, Chatham Maritime, Kent, ME4 4TB, UK; ³UKUK Dementia Research Institute, University College London, Gower Street, London WC1E 6BT.

*Correspondence: Elinor P. Thompson, te30@greenwich.ac.uk

Keywords: CO₂-concentration mechanism; FtsH; mixotrophy; rhomboid protease; serine protease; *Synechocystis*.

Abbreviations: CCM, carbon-concentrating mechanism; DCMU, 3-(3,4-dichlorophenyl)-1,1-dimethylurea; EGF, epidermal growth factor; ER, endoplasmic reticulum; GT, glucose-tolerant; iRhoms, inactive subset of rhomboids; PAM, pulse-amplitude modulation; PSII, photosystem II; TF, transcription factor.

Six supplementary figures and three supplementary tables are available with the online version of this article.

001673 © 2026 The Authors



This is an open-access article distributed under the terms of the Creative Commons Attribution License.

in the case of the *Providencia stuartii* AarA rhomboid protease. In that case, quorum signalling was permitted following AarA activation of the membrane-located TatA component of the Tat transport channel by cleaving the N-terminal six amino acids [5].

Rhomboid proteases are atypical serine proteases whose conserved structure of a six- or seven-transmembrane domain core contains only a catalytic dyad, comprising Ser and His without the usual third active-site residue, Asp [6, 7]. Whereas crystal structures were resolved for the *Haemophilus influenzae* and *Escherichia coli* bacterial enzymes, the roles of prokaryotic rhomboids are only slowly being elucidated [8]. A hypothesis that *E. coli* GlpG may facilitate fatty acid utilization, enhancing survival in intestinal mucus [9], does correspond with other links between rhomboids and lipids. For example, both the *Corynebacterium glutamicum* [10] and *Shigella sonnei* rhomboid pairs were suggested to affect membrane quality control [11], whereas two organellar rhomboid proteases were hypothesized to regulate membrane-fusion dynamics, in the mitochondria of *Saccharomyces cerevisiae* and *Drosophila melanogaster* [12, 13].

Another eukaryotic, organellar representative is the presenilin-associated rhomboid-like protease of the inner mitochondrial membrane, an enzyme that operates within human mitochondrial-disease networks [14]. Rhomboid proteins also have medical significance in their regulation of host-cell infection in the apicomplexan genera *Toxoplasma* and *Plasmodium* [15, 16].

A catalytically inactive subset of rhomboids (iRhoms, or pseudoproteases), which lack protease active-site residues, can still play roles in signal transduction. For example, overexpression of *Drosophila* iRhom inhibited EGF receptor-mediated signalling [17], whereas human iRhom2 is required for trafficking and activation of the TNF- α -converting enzyme for TNF signalling [18].

One or two rhomboid genes, only, tend to be found within prokaryotic genomes, whereas plant genomes encode multigene families of the proteases [19], but few, again, have been studied. Given the prokaryotic origin of eukaryotic organelles, investigating the chloroplast or mitochondrial rhomboid proteases of plants might allow evolutionary links in the enzyme family to be revealed. This type of parallel study was useful for chloroplast versus cyanobacterium FtsH-family membrane proteases, with *Arabidopsis thaliana* VAR2 and *Synechocystis* sp. PCC 6803 Slr0228 (FtsH2) enzymes, both discovered to be operating in the photosystem II (PSII) D1 protein replacement cycle [20, 21]. Compared with four of 12 FtsH enzymes thought to function in *A. thaliana* plastids [22, 23], 3 of about 20 rhomboid proteins in the plant have been demonstrated to be targeted to organelles. In transient assays, *Arabidopsis* At1g18600 (RBL12) was observed in the mitochondria, although this protein did not complement yeast mitochondrial rhomboid mutant function [24]. *Arabidopsis* At5g25752 (RBL11) was directed to the chloroplast [25], where it was hypothesized to function in plastid-protein translocation [26]. A stably transformed RBL10-GFP reporter was visualized in the chloroplast outer membrane, and *rbl10* null-mutants demonstrated floral abnormalities, reduced fertility and a photosynthetic phenotype correlated with increasing light intensity [27].

Identifying cyanobacterial rhomboid proteases was of interest because much of their photosynthetic machinery is conserved in plant chloroplasts. As above, these oxygenic photoautotrophs were already found to share some proteolytic mechanisms, but aquatic cyanobacteria encounter distinct environmental challenges. One such is the acquisition of carbon dioxide, which diffuses poorly in water [28]. Cyanobacteria have overcome this constraint, which coexists alongside the imperfect affinity of ribulose biphosphate carboxylase-oxygenase (RubisCO) for CO₂ and its wasteful side reaction with oxygen [29], through the evolution of a specialized carbon-concentrating mechanism (CCM). Carboxysome 'organelles' house the cyanobacterial RubisCO [30–32] and enrich the CO₂ environment. Because the CCM is energy-dependent, it is regulated at multiple levels, including transcriptional control of CO₂-uptake genes (for review, see [33]). Regulatory components include both activator and repressor transcription factors [34] and, notably, proteolysis of the central NdhR transcription factor (TF) by FtsH2 [35].

Here, mutant cells lacking the Slr1461 rhomboid protease were observed to aberrantly regulate oxygen evolution during mixotrophic growth, when the need for carbon fixation from CO₂ was reduced. The possibility of this rhomboid protease affecting the regulation of the CCM, in addition to the activity of the FtsH protease, was considered by investigating transcription of CCM TF genes, including NdhR, CmpR and an AbrB family member in Δ *slr1461* *Synechocystis*. Whereas there was no indication of transporters being misregulated at the level of steady-state mRNA, the Δ *slr1461* rhomboid-null mutant exhibited altered levels of TF transcripts when CO₂ concentrations were raised. There is increasing interest in TF activated by proteolytic cleavage in other systems [36], and transcriptional links also found between *slr1461* and *ftsH2* were intriguing when considered alongside a recent report of a *Bacillus* bacterial rhomboid cooperating with FtsH in degradation of a transporter protein [37]. This study of the *Synechocystis* rhomboid, therefore, adds a further protein regulator to control networks for bacterial oxygenic photosynthesis and provides a route for further study of coordinated proteolysis events.

METHODS

Inactivation of *Slr1461*

Glucose-tolerant (GT) *Synechocystis* sp. PCC 6803 cells from 25 to 50 ml cultures in the exponential growth phase (OD₇₅₀ ~0.5) were harvested by centrifugation, resuspended in 100 μ l fresh BG11 medium [38] and mixed with 1–2 μ g of plasmid DNA for insertional inactivation by homologous recombination of an antibiotic-resistance gene-interrupted *slr1461*

ORE. Following incubation at 30 °C for 4 h at 8 $\mu\text{mol photons m}^{-2} \text{s}^{-1}$ in a stationary illuminated incubator, with occasional inversion of the tube, cells were plated onto non-selective BG11-agar and incubated overnight. After 24 h, plates were overlaid with 3 ml of 0.6% agar containing selection antibiotic (i.e. 15 μl of 100 mg ml^{-1} kanamycin per 3 ml of 0.6% agar). Antibiotic-resistant transformants were picked as single colonies after ~2 weeks and plated on fresh selective agar plates at least twice to ensure homoplasmicity of the polyploid genome before confirming this by PCR (Fig. S1, available in the online Supplementary Material). The pEERM4 vector (Addgene plasmid #64026), which integrates into the chromosomal neutral site 2, was used to construct the *Slr1461* complementation plasmid. pEERM4 plasmid contains a nickel-inducible rnsB promoter [39]. The full-length *slr1461* coding sequence was cloned into pEERM4 using *XbaI* and *PstI* restriction endonucleases to generate pEERM_Slr1461. This construct was subsequently transformed into the $\Delta\text{slr1461}$ mutant to enable integration at neutral site 2.

Oxygen evolution

Synechocystis 6803 [glucose-tolerant (GT)] cells were harvested once they reached an OD_{750} of ~0.4–0.5 by centrifuging at 2,000 g for 5 min at room temperature (22 °C) and were then adjusted to an OD_{750} of ~0.5 with fresh BG11 medium. For mixotrophic cultures, the pellet was resuspended in fresh BG11 medium containing 5 mM glucose. NaHCO_3 was added to a final concentration of 10 mM, 5 min before the start of measurements. The rates of net O_2 evolution and dark respiration were then measured [40] at 30 °C using a Clark-type electrode (Hansatech, Kings Lynn, UK [41]). Sodium dithionite was used to calibrate the electrode. Actinic light was provided using a 650-nm red LED light. Variable light intensity was set for 0–2300 $\mu\text{mol photons m}^{-2} \text{s}^{-1}$. After an initial 30-min dark adaptation, O_2 evolution was measured for 5 min, followed by dark respiration for 20 min. The mean net rate of photosynthesis was then determined from the oxygen gradient over 5 min. Dark respiration was determined by following the same procedure, except that it was calculated with data from the last 5 min of the 20 min experiment.

Room temperature fluorescence

Maximum quantum yield of PSII was measured using a Walz (Effeltrich, Germany) pulse-amplitude modulation (PAM) 101 fluorimeter with the 101-ED emitter-detector unit. A Walz liquid cell adaptor maintained at 30 °C was used to contain the sample. Actinic light was white light (50 $\mu\text{mol photons m}^{-2} \text{s}^{-1}$) behind a 420-nm Corning 4–96 glass filter (cut-on wavelength at 600 nm). Far-red light was provided by PAM-102. Prior to measurement, cells were harvested as before and concentrated to 10 $\mu\text{g ml}^{-1}$ chlorophyll and dark-adapted for 5 min. Minimum fluorescence (F_0) was determined by illuminating with measuring light (0.01 $\mu\text{mol photons m}^{-2} \text{s}^{-1}$). Maximum fluorescence (F_m) for the dark-adapted state was determined with a 0.8 s long saturation (4500 $\mu\text{mol photons m}^{-2} \text{s}^{-1}$) pulse delivered from a Schott (Elmsford, USA) KL 1500 white light source. The actinic light was then switched on and a second saturation pulse was applied after 5 min (F'_m). Finally, maximum fluorescence (F_m) was determined following the injection of 3-(3,4-dichlorophenyl)-1,1-dimethylurea (DCMU) at a 10 μM final concentration to inhibit electron transport from PSII while actinic light was on [42].

Low-temperature fluorescence

77 K fluorescence emission spectra from the WT and $\Delta\text{slr1461}$ insertional inactivation mutant were recorded in liquid nitrogen using a Perkin Elmer (Waltham, MA, USA) LS 55 luminescence spectrometer. All samples were dark-adapted for 5 min before freezing. The excitation was 440 nm and 580 nm (5 nm slit width), and the fluorescence emission was scanned in a wavelength range of 600–750 nm.

Growth assays

Synechocystis 6803 (GT) cultures were treated with 2.5 μM NiCl_2 and incubated at 30 °C for 3 h with shaking to induce *slr1461* gene expression in the complemented strain. For consistent growth conditions, the four replicates of WT and $\Delta\text{slr1461}$ cells were also treated with 2.5 μM NiCl_2 as above. The cells were then diluted ~22-fold to an OD_{750} of 0.1 in 50 ml BG11 medium containing 5 mM glucose and incubated at a light intensity of 16, 81 or 150 $\mu\text{mol photons m}^{-2} \text{s}^{-1}$ for ~6 days. A 1 ml sample was removed every 24 h for analysis. Specific growth rate (μ) and doubling time (Td) of all cultures were calculated according to the recorded OD_{750} by the photospectrometer (Lambda U3900; Hitachi) according to:

$$\mu = \frac{\ln \text{OD}_t - \ln \text{OD}_0}{\Delta t}$$

$$\text{Td} = \frac{\ln 2}{\mu}$$

where OD_t and OD_0 refer to optical density at time t (h) and time zero, respectively. Chlorophyll content was determined by subtracting the OD_{750} nm value from the OD_{680} nm value and multiplying the result by 10.854, as previously described [43].

RNA isolation and quantitative real-time PCR

Four independent cultures of each strain were grown at a light intensity of 30 $\mu\text{mol photons m}^{-2} \text{s}^{-1}$ in 'low' CO_2 (i.e. normal atmospheric levels) conditions to an OD_{750} of 0.4–0.5. Samples were either treated with 5 mM glucose (for mixotrophic growth), bubbled with 5% CO_2 (raised CO_2 condition) or left untreated (low CO_2 condition). After 6 h, 40 ml samples were collected and pelleted at 3,000 g before being stored at -80°C for RNA extraction. Total RNA was extracted with QIAGEN (Hilden, Germany) RNeasy Plant Mini Kit. RNA was treated with DNase I, RNase-free (Merck Life Sciences, Gillingham, UK) to eliminate possible genomic DNA contamination. First-strand cDNA was synthesized from 1 μg of RNA with the RevertAid First Strand cDNA Synthesis Kit (Fisher Scientific, Loughborough, UK). The cDNA was diluted 100-fold, and 1 μl was used in quantitative real-time PCR, performed with PowerUp (Applied Biosystems, Waltham, USA) SYBR green kit. The values for target genes' transcript level were normalized to both total RNA and to housekeeping gene *16S rRNA* (for primer pairs, see Table 1); the relative changes in transcript abundance were analysed using the $2^{-\Delta\text{Ct}}$ method [44, 45].

Sequence analysis

Sequence similarity searching was carried out with BLASTP and BLASTN using the National Center for Biotechnology Information public database (<https://www.ncbi.nlm.nih.gov/>) [46]. Multiple alignments were generated with CLUSTAL OMEGA [47], and alignments were edited with Jalview [48]. Active site and expected transmembrane architecture were predicted using hydropathy plots (TMHMM) [49] and AlphaFold3 [50].

RESULTS

Identification of rhomboid proteases in cyanobacterial lineages

A single rhomboid protease encoded by the *Synechocystis* 6803 genome was identified from sequence searches, and active site and expected transmembrane architecture were predicted (Fig. 1a–c). Almost all sequenced cyanobacterial genomes were found to encode a single rhomboid (Fig. 1d), but there was some variation, notably within the reduced genomes of the *Prochlorococcus* genus. In contrast, the genome of *Acaryochloris marina* MBIC 11017 includes six rhomboid protease genes, four of which were predicted for *Gloeothoece citrififormis* PCC 7424 (also known as *Cyanothece* sp. PCC 7424) and *Leptolyngbya* sp. CCNP 1308 and three in *Trichormus variabilis* ATCC 29413 (previously named *Anabaena varibilis* ATCC 29413), *Nostoc punctiforme* PCC 73102, *Crocospaera subtropica* ATCC 51142 and *Picosynechococcus* sp. PCC 7002 (previously named *Synechococcus* sp. PCC 7002/*Agmenellum quadruplicatum* PR-6). In contrast, *Prochlorococcus marinus* str. MIT 9313 and *Rippkaea orientalis* PCC 8801 were more typical of a fairly common subset predicted to have duplicated rather than single rhomboid representatives. Examples of cyanobacterial genomes that have evolved rapidly over evolution and lost their rhomboid gene were found to include *Thermosynechococcus elongatus* BP-1, *Trichodesmium erythraeum* IMS101 and

Table 1. Primer pairs used in quantitative real-time PCR and *slr1461* complementation

For quantitative real-time PCR
slr1461_F: TCTTTGCACCCTTTCTCCAT slr1461_R: TTTGGAACCAACCTCGAAAG
ftsH2_F: GCAAGTTAGCGACCCAGAAG ftsH2_R: CCCACAAAACCCAAACCAT
sbtA_F: TGGTGCTCTGTATCCCTTTATG sbtA_R: TGCTGAACGATTCTCAATACT
ndhF3_F: TTTGGCCTTAATTGCTGGAC ndhF3_R: GCGATCGCAATTAAAGAAGC
16S rRNA_F: CACACTGGGACTGAGACAC 16S rRNA_R: CTGCTGGCAGGAGTTAG
abrB2_F: CTGCCCCGGTCAATATGAT abrB2_R: TTGGATTGCACGCTAATGCG
cmpR_F: GTGATTGCTGACCTCCAGGG cmpR_R: CCCAAAAGTCGTGGCACAAA
For complementation
slr1461_F: CTCTAGACCACCATGAGCCAAAATTCC slr1461_R: CTGCAGTGCTAATTTTGTCTGTAGTAATGC

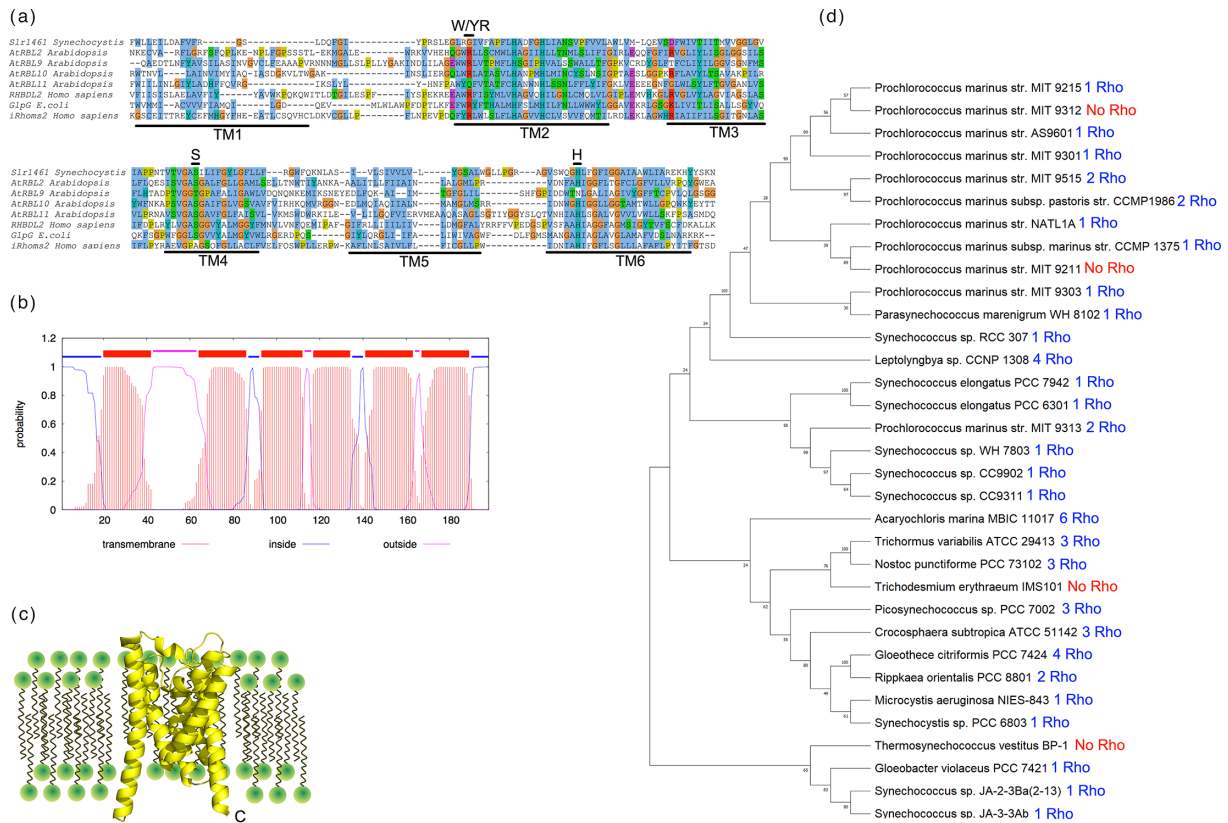


Fig. 1. Slr1461 motifs for rhomboid catalytic activity. (a) Slr1461 aligned with plant and human rhomboid aa sequences. Colour, aa chemical properties and degree of conservation (standard CLUSTALX scheme [47]): purple, acidic amino acids; blue, hydrophobic; green, polar and neutral; brown, glycine; khaki, proline). Segments of sequences aligned are from predicted full-length proteins as follows: *Synechocystis* Slr1461 aa27–196; *A. thaliana* enzymatically active rhomboids RBL2, aa64–252/plastid RBL9, aa275–375/plastid RBL10, 128–310/plastid RBL11, 85–272; *H. sapiens* catalytically active RHBDL2, aa73–273; *H. sapiens* catalytically inactive iRhom2, aa605–796; and *E. coli* GlpG, aa97–276. Bar above sequence alignment indicates conserved aa W/Y/R, S and H. (b) Slr1461, Predicted transmembrane domains (TMHMM) [49]. (c) AlphaFold 3-predicted structure of full-length *Synechocystis* sp. PCC 6803 Slr1461 protein [50]. (d) Distribution of rhomboid proteases in cyanobacteria: unrooted phylogenetic tree for 16S rRNA generated using the neighbour-joining method. The presence or absence of rhomboid (Rho) protein in each cyanobacterial strain is shown on the right. 'No Rho', absence of rhomboid protein.

P. marinus str. MIT 9312 and MIT 9211 [51], in tandem with a reduced complement of genes for regulatory components such as sigma factors, required for transcription initiation, light sensors/transducers and two-component sensor-kinases [51].

Synechocystis rhomboid sequence features

The *Synechocystis* 6803 rhomboid gene, ORF *slr1461*, translates to an amino acid sequence with 37% and 26% identity to the *A. thaliana* chloroplast rhomboids At5g25752/RBL11 and At1g25290/RBL10, respectively. It also shows 28% identity with the endoplasmic reticulum-localized At1g63120/RBL2, but no significant similarity was found with the mitochondrial At5g38510/RBL9.

To predict whether the Slr1461 protein was likely to be enzymatically active or was an inactive iRhom-type rhomboid, its sequence was aligned with representative enzymes already experimentally verified to be catalytically active from *A. thaliana* [52], *Homo sapiens* and *E. coli* [53] and against the catalytically inactive *H. sapiens* iRhom2 rhomboid protease [54, 55] (Fig. 1a). The Slr1461 sequence aligned well with catalytically active rhomboids across transmembrane domains, with clearly conserved active-site serine and histidine residues (Fig. 1a) [56]. These residues were similarly conserved in the active *A. thaliana* rhomboid family (At1g63120/RBL2, mitochondrial At5g38510/RBL9 and chloroplast-located At1g25290/RBL10), *H. sapiens* RHBDL2 and *E. coli* GlpG. Although the overall sequence of human iRhom2 also aligned reasonably well (25% identity between Slr1461 and iRhom2), its corresponding positions lack these catalytic residues, consistent with iRhom2's known enzymatic inactivity [18]. Slr1461, therefore, displays features of the catalytically active rhomboids. It is worthy of note, however, that it lacks a commonly conserved rhomboid N-terminal

tryptophan–tyrosine/arginine (W/YR) motif (Figs 1a and S2) [55, 57], Which was hypothesized at one time to influence the rate of proteolysis [58].

Photosynthesis phenotype

The *A. thaliana* chloroplast *RBL10* mutant's significantly higher NPQ values than in WT plants, correlated with increasing light intensity [27], prompted exploration of a range of photosynthetic parameters in $\Delta slr1461$ *Synechocystis*. Whole-cell absorbance spectra of $\Delta slr1461$ and WT cells were broadly similar under low-intensity light (Fig. 2), but spectra normalized to the phycocyanin peak (635 nm) revealed a slightly higher absorbance at 687 nm in $\Delta slr1461$, consistent with an increased chlorophyll a contribution relative to phycobiliproteins. Quantification of pigment confirmed that $\Delta slr1461$ cultures contained significantly higher total chlorophyll a than WT ($\Delta slr1461$ mean \pm SEM, $8.7\pm 0.51\ \mu\text{M}$ vs. WT $6.1\pm 0.08\ \mu\text{M}$; t-test $P=0.024$, 7 d.f.), supported by ANOVA (see below, Table 2). Oxygen evolution in low light-grown *Synechocystis* WT vs. $\Delta slr1461$ cells was not significantly different if cultures were grown in standard BG11 autotrophic medium with saturating bicarbonate (Fig. 3a). Likewise, the PAM fluorometry assays of $\Delta slr1461$ Fv/Fm, PSII efficiency and NPQ produced measurements not significantly different from WT under low-intensity light conditions (Table 3).

GT *Synechocystis* strains are useful for mutant studies because genes encoding key photosynthetic components can be knocked out, but cultures are able to remain viable [59] if the BG11 defined medium is supplemented to permit heterotrophy. GT cells can, therefore, acquire inorganic carbon either from CO_2 during autotrophic growth or, alternatively, from both glucose and CO_2 in mixotrophic growth. The measurement of oxygen evolution rate under such mixotrophic conditions revealed the most distinct phenotype for glucose-tolerant $\Delta slr1461$ *Synechocystis*. The rate of photosynthesis, previously identical in autotrophic cultures of $\Delta slr1461$ and WT (Fig. 3a), was regulated down by about a third in WT cells when grown mixotrophically, as expected. This reduction, however, did not occur in mixotrophic $\Delta slr1461$ cells (Fig. 3b). Importantly, dark respiration rates were comparable

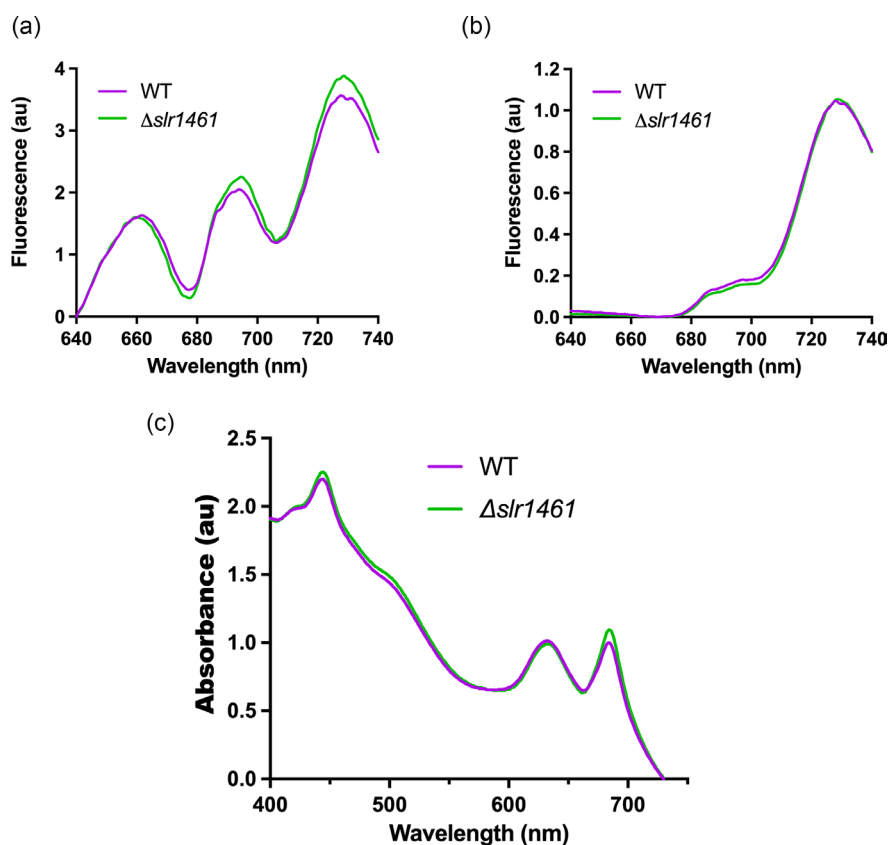


Fig. 2. Photosystems and pigments in 77K fluorescence emission and absorption spectra of mixotrophic WT vs $\Delta slr1461$ cells. (a) 77K spectra normalized to the emission band at 650 nm (580 nm excitation); (b) 77K spectra normalized to the emission band at 725 nm (440 nm excitation); (c) absorption spectra normalized at 687 nm. Maximum absorbance at 448 nm, 635 nm and 687 nm corresponds to carotenoid, phycocyanin and chlorophyll peaks, respectively. Cultures for A-C grown in BG11 medium supplemented with 5 mM glucose at $8\ \mu\text{mol photons m}^{-2}\ \text{s}^{-1}$ light. Green line, $\Delta slr1461$; purple line, WT *Synechocystis* sp. PCC 6803.

Table 2. Two-way ANOVA to analyse the effects of WT vs. $\Delta slr1461$ genotype and light intensity, and their interaction, on doubling time and chlorophyll a (Chl a) content

	Genotype			Light intensity			Genotype vs light intensity		
	Df	F	p	Df	F	p	Df	F	p
Doubling time	2	3.2	0.0551	2	30	<0.0001	4	1.9	0.1287
Chl a	2	51	<0.0001	2	17	<0.0001	4	1.0	0.3927

Data were transformed (log, square root or reciprocal) as needed to meet linear model assumptions. Df, degrees of freedom; F, variation between sample means; p, significance levels.

between the mutant and WT strains (Fig. S5), indicating that the observed differences in O₂ evolution under mixotrophy reflected changes in photosynthetic regulation rather than respiratory activity.

As cyanobacteria divide more rapidly in the presence of glucose [60], a marked difference like this in photosynthetic activity (Fig. 3b) might arise if there was a defect in glucose import in the absence of the Slr1461 rhomboid. Growth rates of the strains did not suggest altered nutrient acquisition; however, statistical analysis using two-way ANOVA (Table 2, Fig. S4) confirmed that, whereas increasing light intensity significantly affected both doubling time ($F=30$, $P\leq 0.0001$) and chlorophyll a content ($F=17$, $P\leq 0.0001$), the genotype (i.e. mutant vs WT) only influenced chlorophyll a ($F=51$, $P=0.0001$), with the lack of Slr1461 having little effect on doubling time ($F=3.2$, $P=0.0551$). A check on experimental conditions showed there was no significant interaction between genotype and light intensity ($P>0.12$).

Genetic regulation of CO₂ concentration components

Mutant $\Delta slr1461$ cells failed to downregulate photosynthesis under mixotrophic growth, when a decrease in photosynthetic activity would normally be observed in *Synechocystis* strains that are capable of heterotrophy. The reduced photosynthesis in WT GT cells follows a decrease in the rate of bicarbonate uptake [61] and metabolic regulation that reduces the activity of the carbon-fixing enzyme, RuBisCO [62]. A hypothesis that lack of Slr1461 resulted in altered behaviour of the CCM was, therefore, tested by quantifying the steady-state mRNA of *slr1461* and of key CCM genes.

Whether the cyanobacterial rhomboid protease itself was regulated at the level of transcript abundance under high CO₂ conditions was investigated by quantifying *slr1461* mRNA level in WT *Synechocystis* (Fig. 4a). *slr1461* transcript level did indeed increase when cultures were bubbled with 5% CO₂, when cells also had higher chlorophyll a content than did WT, as noted previously (Table 2). These data indicated that the Slr1461 protease may be involved in the regulation of carbon assimilation.

Genes encoding components of the CCM were tested, therefore, during adaptation of $\Delta slr1461$ cultures to high CO₂ or to mixotrophic conditions, to assess their transcription levels when carbon fixation demand was reduced (Fig. 4, Table S2).

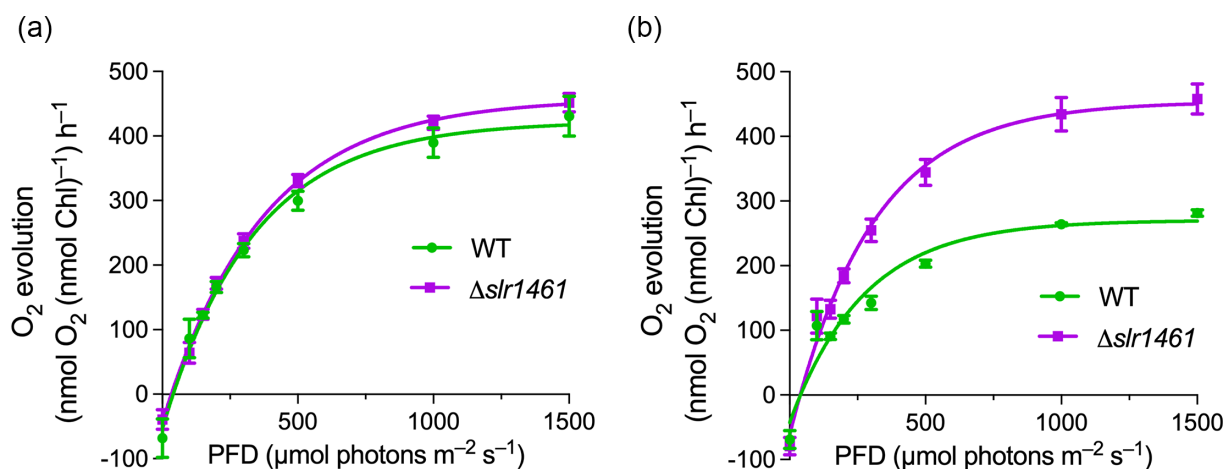


Fig. 3. Light-response curve for WT vs. $\Delta slr1461$ cells. Oxygen evolution rate versus photon flux density (PFD) for autotrophic (a) vs. mixotrophic (b) cultures grown at $8 \mu\text{mol photons m}^{-2} \text{s}^{-1}$ light. Cells grown mixotrophically were supplemented with 5 mM glucose. Net photosynthesis rate (measured as in the 'Methods' section) datapoints are the mean of three measurements \pm SEM. For statistics, an unpaired Student's t-test was performed. Asterisks, Statistically significant changes (P -value < 0.05).

Table 3. Photosynthesis in the *Synechocystis* $\Delta slr1461$ rhomboid protease mutant

	Autotrophic				Mixotrophic				High light autotrophic			
	F_v/F_m	F_v/F_m DCMU	Φ_{PSII}	NPQ	F_v/F_m	F_v/F_m DCMU	Φ_{PSII}	NPQ	F_v/F_m	F_v/F_m DCMU	Φ_{PSII}	NPQ
WT	0.38(±0.04)	0.56(±0.01)	0.35(±0.02)	0.25(±0.02)	0.30(±0.03)	0.49(±0.01)	0.20(±0.06)	0.13(±0.06)	0.26(±0.02)	0.32(±0.02)	0.14(±0.03)	0.09(±0.01)
$\Delta slr1461$	0.37(±0.02)	0.58(±0.0)	0.37(±0.04)	0.26(±0.02)	0.32(±0.04)	0.49(±0.03)	0.17(±0.06)	0.13(±0.06)	0.31(±0.00)	0.36(±0.01)	0.13(±0.01)	0.10(±0.02)

Pulse-modulated chlorophyll fluorescence measurements of quantum yield of photosystem II (PSII): photochemical quantum yield F_v/F_m for dark-adapted cells was calculated from $(F_m - F_o)/F_m$. Maximum quantum yield of PSII (F_v/F_m DCMU) was measured using a protocol employing continuous illumination in the presence of 10 μ M DCMU. The effective quantum yield of PSII (Φ_{PSII}) was calculated as $(F_m - F_o)/F_m$, and non-photochemical quenching (NPQ) was calculated from $(F_m - F_m)/F_m$. Results are means from three biological measurements \pm sd.

The *sbtA* gene, encoding the Na^+ -dependent HCO_3^- transporter, was aberrantly low under all conditions in $\Delta slr1461$: for example, the mutant had a \log_2 -fold *sbtA* level of -0.63 ($P=0.014$) vs WT under standard (lower) CO_2 conditions, moving to a -1.01 \log_2 -fold value ($P=0.015$) under 5% (raised) CO_2 (Fig. 4b, Tables S2 and S3).

Also aberrant was the transcript for the NdhF3 protein, a component of the cyanobacterial high-affinity CO_2 uptake system (comprising a complex of NdhD3/D4 and NdhF3/F4), which catalyses CO_2 uptake by converting CO_2 into HCO_3^- . In this case, in mixotrophic $\Delta slr1461$ cultures, *ndhF3* mRNA levels in the mutant were similar to those in WT (Table S2). In autotrophy, however, under normal atmospheric CO_2 conditions, *ndhF3* mRNA \log_2 -fold levels were -5.90 and in raised CO_2 conditions were -4.57 (Fig. 4a, Table S2), i.e. lower than in $\Delta slr1461$ than in WT in both conditions. Likewise, *slr1461* itself had been observed to accumulate only under raised CO_2 , and not under mixotrophic glucose-supplemented conditions (Fig. 4a, Table S2), a CO_2 -dependent regulation of *slr1461* was reported before [33]. Therefore, the lack of difference in *ndhF3* transcript level between WT and $\Delta slr1461$ mutant in mixotrophic growth can be attributed to the absence of *slr1461* transcripts. When Slr1461 is not expressed (i.e. in mixotrophy), its regulatory influence on NdhF3 expression is lost.

Other CCM components examined were CmpR and an AbrB family member. Both *abrB2* and *cmpR* were also aberrantly regulated when Slr1461 was lacking, being significantly lower in the $\Delta slr1461$ mutant than WT when cultures were subject to increased CO_2 (Fig. 4b, Table S2), although their levels were little different in $\Delta slr1461$ to WT under lower CO_2 levels.

Coordinate control of CCM by proteases

It was previously reported that induction of *ndhF3* and *sbtA* requires the FtsH2 protease as these CCM transcripts were not upregulated under low CO_2 conditions in a null mutant with inactivated *ftsH2* [35]. Meanwhile, increased *ftsH2* transcript levels have been reported either in response to oxidative stress; not to change in a shift from high to low CO_2 [35]; or with a very minor upregulation in transcript under CO_2 downshift in an earlier study [33]. The presence of the FtsH2 protease in networks connected with CCM regulation was further monitored in WT compared with $\Delta slr1461$ cells, comparing *ftsH2* transcript levels in standard or raised CO_2 conditions in this mutant. Notably, after increasing CO_2 levels, the *ftsH2* transcript level in $\Delta slr1461$ remained lower than in WT cells (Fig. 4b, Table S2), indicating that Slr1461 presence or proteolytic activity may affect induction of the *ftsH2* gene in WT cyanobacteria.

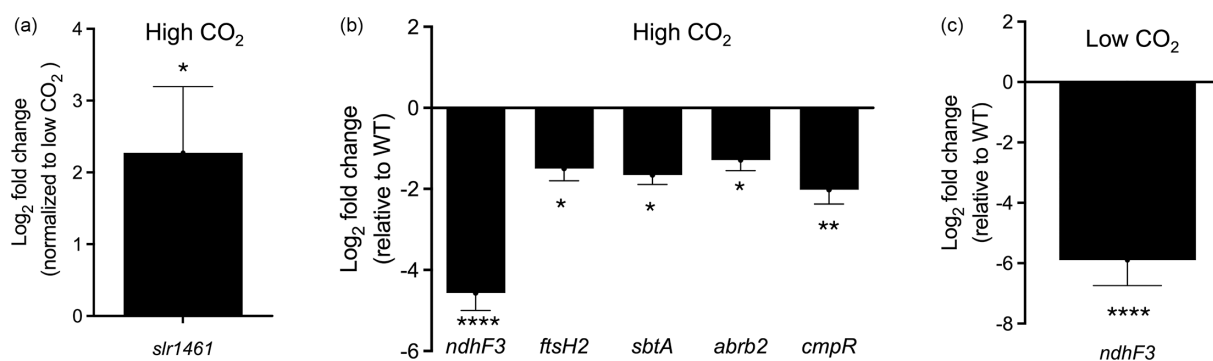


Fig. 4. Effect of high CO_2 on CCM gene transcript level in (a) WT or (b, c) $\Delta slr1461$ compared with WT. Strains grown in atmospheric-level CO_2 (low CO_2) at $30 \mu\text{mol photons m}^{-2} \text{s}^{-1}$ light intensity until OD_{750} of 0.4–0.5, after which they were bubbled with 5% CO_2 (high CO_2) or left untreated before further 6 h incubation. Quantitative real-time PCR on extracted RNA permitted calculation of expression levels relative to 16S rRNA reference gene, with further normalization to the WT (Fig. 4b–c, Table S2). Statistical significance (P -value ≤ 0.05), denoted by * ≤ 0.05 , ** 0.01 and **** 0.0001 . For a complete list of P -values, see Table S3.

To confirm that the decrease in CCM genes' transcript levels resulted from the absence of Slr1461 activity, the *slr1461* gene was used to complement Δ *slr1461* cells. In the complemented line, *slr1461*, *ftsh2* and *ndhF3* transcript levels were rescued (Fig. S6). The regulatory changes here suggested that further exploration is warranted to elucidate precisely the role of Slr1461 in connection with CCM processes.

DISCUSSION

Given their evolutionary relationship with plastids, cyanobacterial predicted rhomboid proteases were examined (see Fig. S3) to compare features and conserved photosynthesis-related roles. This first experimental investigation into the function of a cyanobacterial rhomboid protease utilized the single rhomboid identified in the genome of the model oxygenic photosynthetic prokaryote *Synechocystis*, with reference to the homologous RBL10 protease of the *A. thaliana* chloroplast. Early literature upon discovery of this protein family reported the most common occurrence in prokaryotic genomes was of a single rhomboid enzyme, as identified in *Synechocystis*, but, subsequently, it has become clear that there are many cyanobacterial genera whose genomes encode multiple copies [63]. BLAST searches of more recently sequenced genomes in fact found many bacteria with duplicated rhomboid genes: the cyanobacterial genera documented here include those encoding as many as six copies (Fig. 1d). This mirrors another group of membrane proteases, where a single FtsH protease regulates many processes in *E. coli* [7] in contrast with the four FtsH copies of both *Synechococcus* sp. PCC 7502 and *Synechocystis* sp. PCC 6803 [20, 64, 65], whose shared and specific roles are integral to oxygenic photosynthesis [20, 21]. Phylogenetic analysis of rhomboid proteins in cyanobacteria showed that species encoding multiple representatives have highly similar sequences indicative of gene duplication, except for the *Acaryochloris marina* genome, which, despite the presence of six rhomboids, contains divergent genes that appear more distinct from one another (Fig. S3). Further dissection of the cyanobacterial single-copy versus multiple-copy rhomboids' roles might provide insight into how a handful of organisms (such as *P. marinus* subspecies) have been able to function without their rhomboid protease (Fig. 1d) despite this protein family's near-ubiquity across evolution.

The *Synechocystis* Slr1461 amino-acid sequence shows good overall alignment with other organisms' rhomboid proteases that are known to be catalytically active. Slr1461 contains the nucleophile Ser and acceptor His required for proteolytic attack of substrate (Fig. 1), but it lacks the W/YR motif often conserved near rhomboid proteases' N-termini (Figs 1a and S2). This motif was initially postulated to play a role in substrate gating but has since been ruled out as the mechanism of capture [58], and its link with enzymatic activity is now questioned. As the presence of conserved active-site serine and histidine suggests a catalytically active protease, this rhomboid may in fact be an interesting candidate for investigations of rhomboid proteolysis in the presence or absence of the W/YR motif [66, 67]. The observed phenotypes following the Δ *slr1461* insertional inactivation mutant also support a hypothesis of Slr1461 being a proteolytically active enzyme, but it must be noted that regulatory roles for inactive rhomboids are plausible in bacteria [68], since an 'adaptor' function was reported for the *Bacillus* enzyme when acting in concert with an FtsH [37].

The constructed *Synechocystis* Δ *slr1461* mutant line was investigated for a range of photosynthetic parameters because of the plastid membrane location of the homologous *A. thaliana* rhomboid RBL10 and the *RBL10* null mutant's light-intensity-dependent raised NPQ [27]. No dramatic difference was identified, however, in Δ *slr1461* cells' pigment-photosystem composition (Fig. 2). Furthermore, there was no difference in NPQ under light conditions tested (Table 3), despite that aspect of the *A. thaliana* *RBL10*-null phenotype. The most dramatic difference observed with the lack of Slr1461 was higher oxygen evolution compared with WT when cells were grown mixotrophically, i.e. with insufficient glucose for full heterotrophy (Fig. 3b). Given that the *Bacillus* rhomboid-FtsH cooperative function was reported to regulate a transporter, namely MgtE of *Bacillus subtilis* [37], the question was prompted over possible defective transport of glucose in the Δ *slr1461* cells. Since glucose typically increases growth rates and alters photosystem composition, the absence of any significant difference in these parameters between mutant and WT cultures under mixotrophic conditions (Table 2, Fig. S4) ruled out this possibility.

Since rhomboid proteases have often been reported to activate or release peptides involved in signalling, the misregulation of Δ *slr1461* carbon utilization could result from a role for the Slr1461 protease in activating the regulatory pathways that control the complex variations needed for cyanobacterial CO₂ uptake and C fixing. It was reported before that numerous CCM components' transcript levels respond to CO₂ [33, 35], which proved to be the case here: several CCM-gene transcript levels were increased in WT cultures moved to high-CO₂ (Fig. 4a), amongst them the *slr1461* transcript. Changes in levels tallied with those reported previously when cells were moved from higher to lower CO₂ and with a small *slr1461* transcript-level change found when the *ftsh2* transcript was upregulated [33]. To integrate data from literature reports, further investigation of the magnitude and direction of changes is needed, ensuring consistent and duplicated culture conditions and CO₂ levels.

Studies in prokaryotes to date only once implicated rhomboid proteases in the regulation of transcript levels [10], namely for the transcription factor (RipA, *cg1120*) involved in iron homeostasis in *C. glutamicum* [10]. Certainly, the release of eukaryotic ER-bound transcription factors is an attractive hypothesis for the roles of this protease family, for which some experimental evidence is accumulating [1, 69–71]. A relevant observation about cyanobacterial carbon assimilation, then, was that the cAMP-regulated TF SyCRP1, which affects carboxysome formation (as well as many other pathways), can be released from a membrane

location [72]. That possible addition to the expanding CCM regulatory map also supports a recent statement that, although the CCM is well characterized, its regulation is complex and not yet fully understood [73].

A study in *Synechocystis* already showed that the FtsH2 protease was involved in the CCM [35], in addition to its well-known role in turnover of the PSII D1 protein [20]. It was proposed that this FtsH degrades the TF, NdhR, that is required for the induction of CCM genes [35]. It is notable how functional photosynthesis was required for the induction of CCM [34] in WT cells cultured in low CO₂ conditions, with the suggestion that oxidative stress in the cells might enhance the expression of inducible CCM genes [35]. Conversely, Haimovich-Dayan *et al.* (2011) reported that CCM genes were induced by glucose [74], possibly through the previously mentioned cAMP-dependent TF SyCRP1 [72].

Quantitative PCR assays here showed that loss of Slr1461 affected transcript levels of the high-affinity CO₂ import system (Fig. 4, Table S2), with CCM transport component and *fhsH2* genes all misregulated. Whereas raising the CO₂ levels in cultures mildly

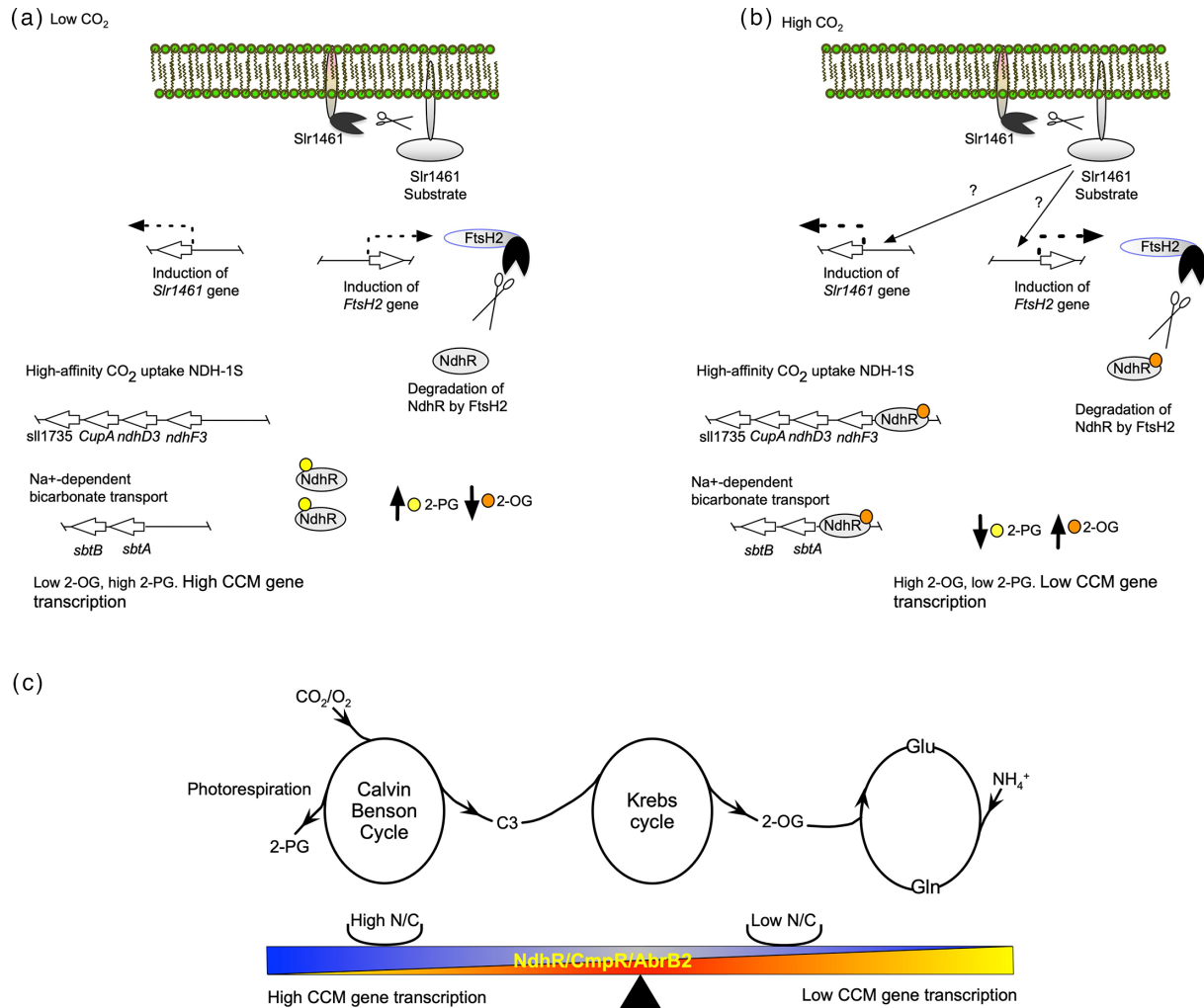


Fig. 5. Proposed further investigation of Slr1461 roles in adaptation of *Synechocystis* to the environment. (a) Under low CO₂ conditions, the oxygenase activity of RuBisCO leads to the accumulation of 2-phosphoglycolate (2-PG) in the cells [81]. The binding of 2-PG to NdhR causes it to be released from the DNA, resulting in an activated transcript level of CCM genes [82]. Meanwhile, NdhR is not degraded in the absence of FtsH2 [35]. (b) High CO₂ levels were correlated with increased transcript level of the *slr1461* gene, which is hypothesized to enhance proteolysis of the rhomboid's as-yet unidentified, activated substrate. This cleaving of the Slr1461-substrate(s) by Slr1461 protease is proposed as a possible mechanism in the pathway for the observed upregulation of *fhsH2* transcript levels. At the same time, 2-oxoglutarate (2-OG) accumulates under high CO₂-low nitrogen conditions: binding of 2-OG to NdhR leads to NdhR adapting to a repressor conformation [82], resulting in repression of CCM genes. (c) Resulting network of coordinated regulation of NdhR, CmpR and AbrB2 by carbon and nitrogen metabolism. The 2-PG and 2-OG levels have opposite effects on the activity of NdhR. Under low CO₂ conditions, the activity of RuBisCO shifts predominantly to the oxygenation of ribulose-1,5-bisphosphate. This, in turn, causes the cell to accumulate 2-PG. 2-OG serves as an intermediate between carbon and nitrogen assimilation, but under high CO₂ conditions, the conversion of 2-OG with ammonium (NH₄⁺) into glutamate is low, resulting in 2-OG accumulation in the cell. The 2-OG and 2-PG molecules are denoted with ● and ○ respectively. Fig. 5C was adapted from [82].

repressed CCM transcription in WT cells, a more marked reduction occurred in the $\Delta slr1461$ mutant (Fig. 4, Table S2). A key observation is how transcript levels of the *ftsh2* gene were affected by the absence of Slr1461, which raises the possibility that the role of the rhomboid protease is to modulate the input of FtsH2 into CCM regulation. A hypothesis then could be that Slr1461 action (its cleaved substrate or its own adaptor function) would permit coordination of the cell's responses to mixotrophic growth and oxidative stress, i.e. an upstream rhomboid protease fine-tunes FtsH regulation of the CCM. Results here (Fig. 4, Table S2) suggested that this proposed Slr1461 activity would specifically affect transcript levels under raised CO₂ conditions, potentially preventing excessive downregulation of CCM genes. The relative position of the proteases and any rhomboid substrate to CCM regulators requires further investigation (Fig. 5). As raised CO₂ levels regulated the *slr1461* transcript level itself, that abiotic factor might likewise regulate the availability of a Slr1461-proteolysed substrate(s). Increased CO₂ in the scheme here could increase either accessibility, degradation or activation of the unidentified Slr1461 substrate, which could have upregulatory or downregulatory functions downstream. A scheme could be that increased CO₂ results in increased transcript levels of *slr1461* and in Slr1461 cleaving its substrate: this also increases the level of *ftsh2*. Notably, FtsH2 metalloprotease upregulation can then increase transcript levels from CCM promoters in higher CO₂ because FtsH2 degrades the NdhR repressor protein [35]. Finally, it is worth mentioning that, since the *ftsh2* gene is induced by oxidative stress in WT *Synechocystis* but not in the stress response histidine kinase *hik33* mutant [35, 75], it would be of interest to explore how the kinase-response regulator Hik33-RpaB abiotic stress mechanism interlinks with this extended CCM regulatory network.

Better knowledge of how photosynthetic organisms respond to CO₂ increases may be useful, underpinning future applications in the capture and storage of the rising CO₂ levels in the atmosphere and oceans resulting from human activity. It has also been suggested that utilizing a cyanobacterial CCM in plants to improve Rubisco efficiency and hence crop yield might not require changes to leaf anatomy [76]. This addition of control by Slr1461 to the FtsH2 release-from-repression of select CCM-related genes [35] would add a mechanism for crosstalk and step-specific feedback. This echoes how proteases of the Clp and Deg families supplement FtsH hetero-oligomers' maintenance of functional PSII in varying environments, which is augmented by phosphorylation controls from kinases and phosphatases [77, 78]. A multilayered response mechanism might likewise be investigated for the CCM. Additionally, as FtsH copies of type 'A' and 'B' can operate as heterodimers (namely FtsH2/3 and FtsH1/3 in *Synechocystis* [23, 79, 80]), another avenue of work would be to identify if upstream Slr1461 rhomboid activity affects more than just the FtsH2 protease. As noted above, in the case of *B. subtilis*, the N-terminal cytosolic domain of rhomboid YqgP facilitates MgtE transporter cleavage by FtsH, by an adaptor function that is separate from any catalytic abilities [37]. Such united protease and pseudoprotease functions add to an increasing body of evidence for proteases' ability to regulate cellular activities by a suite of mechanisms. The diverse rhomboid functions reported to date lack a unifying and evolutionarily conserved framework for their operation, but findings here for the CCM once again support linked roles for rhomboid and FtsH membrane proteases. Further study of this aspect of the cyanobacterial carbon-concentrating system may prove a useful focus for developing our understanding.

Funding information

The University of Greenwich funded E.P.T., B.T.F., D.H. (VC Scholarship), M.B.-H. and I.M.I. and Towson University funded I.M.I.

Acknowledgements

We thank Professor C.W. Mullineaux for help with 77K fluorescence spectra, Dr C. Bateman for help in constructing *Slr1461* knockouts and Dr M. Rafiq for valuable discussions.

Author contributions

I.M.I. and E.P.T. were responsible for the design and analysis of experiments and project management. I.M.I., D.H., M.B.-H., B.T.F. and E.P.T. were responsible for conducting experiments. I.M.I. and E.P.T. conceptualized and wrote the manuscript. All authors have read and agreed to the published version of the manuscript.

Conflicts of interest

The authors declare that there are no conflicts of interest.

References

- Freeman M. The rhomboid-like superfamily: molecular mechanisms and biological roles. *Annu Rev Cell Dev Biol* 2014;30:235–254.
- Urban S, Lee JR, Freeman M. *Drosophila* Rhomboid-1 defines a family of putative intramembrane serine proteases. *Cell* 2001;107:173–182.
- Lee JR, Urban S, Garvey CF, Freeman M. Regulated intracellular ligand transport and proteolysis control EGF signal activation in *Drosophila*. *Cell* 2001;107:161–171.
- Rather P. Role of rhomboid proteases in bacteria. *Biochim Biophys Acta* 2013;1828:2849–2854.
- Stevenson LG, Strisovsky K, Clemmer KM, Bhatt S, Freeman M, et al. Rhomboid protease AarA mediates quorum-sensing in *Providencia stuartii* by activating TataA of the twin-arginine translocase. *Proc Natl Acad Sci USA* 2007;104:1003–1008.
- Ekici OD, Paetzel M, Dalbey RE. Unconventional serine proteases: variations on the catalytic Ser/His/Asp triad configuration. *Protein Sci* 2008;17:2023–2037.
- Tomoyasu T, Gamer J, Bukau B, Kanemori M, Mori H, et al. *Escherichia coli* FtsH is a membrane-bound, ATP-dependent protease which degrades the heat-shock transcription factor sigma 32. *EMBO J* 1995;14:2551–2560.
- Russell CW, Richards AC, Chang AS, Mulvey MA. The rhomboid protease GlpG promotes the persistence of extraintestinal pathogenic *Escherichia coli* within the Gut. *Infect Immun* 2017;85:e00866–16.
- Lu J, Arutyunova E, Hartley B, Wong J, Chung H, et al. Rhomboid protease GlpG regulates type 1 pili quality control and virulence in pathogenic *E. coli*. *Nat Commun* 2025;17.

10. Luenenschloss A, Ter Veld F, Albaum SP, Neddermann TM, Wendisch VF, et al. Functional genomics uncovers pleiotropic role of rhomboids in *Corynebacterium glutamicum* *Front Microbiol* 2022;13:771968.
11. Liu G, Beaton SE, Grieve AG, Evans R, Rogers M, et al. Bacterial rhomboid proteases mediate quality control of orphan membrane proteins. *EMBO J* 2020;39:e102922.
12. Hill RB, Pellegrini L. The PARL family of mitochondrial rhomboid proteases. *Semin Cell Dev Biol* 2010;21:582–592.
13. McQuibban GA, Lee JR, Zheng L, Juusola M, Freeman M. Normal mitochondrial dynamics requires rhomboid-7 and Affects *Drosophila* Lifespan and Neuronal Function. *Current Biology* 2006;16:982–989.
14. Lysyk L, Brassard R, Touret N, Lemieux MJ. PARL Protease: a glimpse at intramembrane proteolysis in the inner mitochondrial membrane. *J Mol Biol* 2020;432:5052–5062.
15. Lin J-W, Meireles P, Prudêncio M, Engelmann S, Annoura T, et al. Loss-of-function analyses defines vital and redundant functions of the *Plasmodium* rhomboid protease family. *Mol Microbiol* 2013;88:318–338.
16. Santos JM, Ferguson DJP, Blackman MJ, Soldati-Favre D. Intramembrane cleavage of AMA1 triggers *Toxoplasma* to switch from an invasive to a replicative mode. *Science* 2011;331:473–477.
17. Zettl M, Adrain C, Strisovsky K, Lastun V, Freeman M. Rhomboid family pseudoproteases use the ER quality control machinery to regulate intercellular signaling. *Cell* 2011;145:79–91.
18. Adrain C, Zettl M, Christova Y, Taylor N, Freeman M. Tumor necrosis factor signaling requires iRhom2 to promote trafficking and activation of TACE. *Science* 2012;335:225–228.
19. Tripathi LP, Sowdhamini R. Cross genome comparisons of serine proteases in *Arabidopsis* and rice. *BMC Genomics* 2006;7:200.
20. Silva P, Thompson E, Bailey S, Kruse O, Mullineaux CW, et al. FtsH is involved in the early stages of repair of photosystem II in *Synechocystis* sp PCC 6803. *Plant Cell* 2003;15:2152–2164.
21. Bailey S, Thompson E, Nixon PJ, Horton P, Mullineaux CW, et al. A critical role for the Var2 FtsH homologue of *Arabidopsis thaliana* in the photosystem II repair cycle in vivo. *J Biol Chem* 2002;277:2006–2011.
22. Friso G, Giacomelli L, Ytterberg AJ, Peltier J-B, Rudella A, et al. In-depth analysis of the thylakoid membrane proteome of *Arabidopsis thaliana* chloroplasts: new proteins, new functions, and a plastid proteome database. *Plant Cell* 2004;16:478–499.
23. Zaltsman A, Ori N, Adam Z. Two types of FtsH protease subunits are required for chloroplast biogenesis and photosystem II repair in *Arabidopsis*. *Plant Cell* 2005;17:2782–2790.
24. Kanaoka MM, Urban S, Freeman M, Okada K. An *Arabidopsis* rhomboid homolog is an intramembrane protease in plants. *FEBS Lett* 2005;579:5723–5728.
25. Kmiec-Wisniewska B, Krumpe K, Urantowka A, Sakamoto W, Pratje E, et al. Plant mitochondrial rhomboid, AtRBL12, has different substrate specificity from its yeast counterpart. *Plant Mol Biol* 2008;68:159–171.
26. Karakasis K, Taylor D, Ko K. Uncovering a link between a plastid translocon component and rhomboid proteases using yeast mitochondria-based assays. *Plant Cell Physiol* 2007;48:655–661.
27. Thompson EP, Smith SGL, Glover BJ. An *Arabidopsis* rhomboid protease has roles in the chloroplast and in flower development. *J Exp Bot* 2012;63:3559–3570.
28. Moroney JV, Ynalvez RA. Proposed carbon dioxide concentrating mechanism in *Chlamydomonas reinhardtii*. *Eukaryot Cell* 2007;6:1251–1259.
29. Moroney JV, Somanchi A. How Do algae concentrate CO₂ to increase the efficiency of photosynthetic carbon fixation? *Plant Physiol* 1999;119:9–16.
30. Giordano M, Beardall J, Raven JA. CO₂ concentrating mechanisms in algae: mechanisms, environmental modulation, and evolution. *Annu Rev Plant Biol* 2005;56:99–131.
31. Kaplan A, Schwarz R, Lieman-Hurwitz J, Reinhold L. Physiological and molecular aspects of the inorganic carbon-concentrating mechanism in cyanobacteria. *Plant Physiol* 1991;97:851–855.
32. Price GD, Badger MR, Woodger FJ, Long BM. Advances in understanding the cyanobacterial CO₂-concentrating-mechanism (CCM): functional components, Ci transporters, diversity, genetic regulation and prospects for engineering into plants. *J Exp Bot* 2008;59:1441–1461.
33. Wang H-L, Postier BL, Burnap RL. Alterations in global patterns of gene expression in *Synechocystis* sp. PCC 6803 in response to inorganic carbon limitation and the inactivation of ndhR, a LysR family regulator. *J Biol Chem* 2004;279:5739–5751.
34. Daley SME, Kappell AD, Carrick MJ, Burnap RL. Regulation of the cyanobacterial CO₂-concentrating mechanism involves internal sensing of NADP⁺ and α -ketoglutarate levels by transcription factor CcmR. *PLoS One* 2012;7:e41286.
35. Zhang P, Sicora CI, Vorontsova N, Allahverdiyeva Y, Battchikova N, et al. FtsH protease is required for induction of inorganic carbon acquisition complexes in *Synechocystis* sp. PCC 6803. *Mol Microbiol* 2007;65:728–740.
36. Jarvis P, López-Juez E. Biogenesis and homeostasis of chloroplasts and other plastids. *Nat Rev Mol Cell Biol* 2013;14:787–802.
37. Began J, Cordier B, Březinová J, Delisle J, Hexnerová R, et al. Rhomboid intramembrane protease YggP licenses bacterial membrane protein quality control as adaptor of FtsH AAA protease. *EMBO J* 2020;39:e102935.
38. Castenholz RW. Culturing methods for cyanobacteria. In: *Methods in Enzymology*. Academic press, 1988. pp. 68–93.
39. Englund E, Andersen-Ranberg J, Miao R, Hamberger B, Lindberg P. Metabolic engineering of *Synechocystis* sp. PCC 6803 for production of the plant diterpenoid manoyl oxide. *ACS Synth Biol* 2015;4:1270–1278.
40. Brindley C, Ación FG, Fernández-Sevilla JM. The oxygen evolution methodology affects photosynthetic rate measurements of microalgae in well-defined light regimes. *Biotechnol Bioeng* 2010;106:228–237.
41. Delieu T, Walker DA. An improved cathode for the measurement of photosynthetic oxygen evolution by isolated chloroplasts. *New Phytologist* 1972;71:201–225.
42. Campbell D, Hurry V, Clarke AK, Gustafsson P, Oquist G. Chlorophyll fluorescence analysis of cyanobacterial photosynthesis and acclimation. *Microbiol Mol Biol Rev* 1998;62:667–683.
43. Lea-Smith DJ, Ross N, Zori M, Bendall DS, Dennis JS, et al. Thylakoid terminal oxidases are essential for the cyanobacterium *Synechocystis* sp. PCC 6803 to survive rapidly changing light intensities. *Plant Physiol* 2013;162:484–495.
44. Andersen CL, Jensen JL, Ørntoft TF. Normalization of real-time quantitative reverse transcription-PCR data: a model-based variance estimation approach to identify genes suited for normalization, applied to bladder and colon cancer data sets. *Cancer Res* 2004;64:5245–5250.
45. Vandesompele J, De Preter K, Pattyn F, Poppe B, Van Roy N, et al. Accurate normalization of real-time quantitative RT-PCR data by geometric averaging of multiple internal control genes. *Genome Biol* 2002;3:Research0034.
46. Altschul SF, Gish W, Miller W, Myers EW, Lipman DJ. Basic local alignment search tool. *J Mol Biol* 1990;215:403–410.
47. Chenna R, Sugawara H, Koike T, Lopez R, Gibson TJ, et al. Multiple sequence alignment with the Clustal series of programs. *Nucleic Acids Res* 2003;31:3497–3500.
48. Clamp M, Cuff J, Searle SM, Barton GJ. The Jalview Java alignment editor. *Bioinformatics* 2004;20:426–427.
49. Krogh A, Larsson B, von Heijne G, Sonnhammer EL. Predicting transmembrane protein topology with a hidden Markov model: application to complete genomes. *J Mol Biol* 2001;305:567–580.

50. Abramson J, Adler J, Dunger J, Evans R, Green T, et al. Accurate structure prediction of biomolecular interactions with AlphaFold 3. *Nature* 2024;630:493–500.
51. Rocap G, Larimer FW, Lamerdin J, Malfatti S, Chain P, et al. Genome divergence in two *Prochlorococcus* ecotypes reflects oceanic niche differentiation. *Nature* 2003;424:1042–1047.
52. Lavell A, Smith M, Xu Y, Froehlich JE, De La Mora C, et al. Proteins associated with the *Arabidopsis thaliana* plastid rhomboid-like protein RBL10. *Plant J* 2021;108:1332–1345.
53. Wang Y, Zhang Y, Ha Y. Crystal structure of a rhomboid family intramembrane protease. *Nature* 2006;444:179–180.
54. Adrain C, Strisovsky K, Zettl M, Hu L, Lemberg MK, et al. Mammalian EGF receptor activation by the rhomboid protease RHBDL2. *EMBO Rep* 2011;12:421–427.
55. Lemberg MK, Freeman M. Functional and evolutionary implications of enhanced genomic analysis of rhomboid intramembrane proteases. *Genome Res* 2007;17:1634–1646.
56. Lemieux MJ, Fischer SJ, Cherney MM, Bateman KS, James MNG. The crystal structure of the rhomboid peptidase from *Haemophilus influenzae* provides insight into intramembrane proteolysis. *Proc Natl Acad Sci USA* 2007;104:750–754.
57. Bergbold N, Lemberg MK. Emerging role of rhomboid family proteins in mammalian biology and disease. *Biochim Biophys Acta* 2013;1828:2840–2848.
58. Zoll S, Stanchev S, Began J, Skerle J, Lepšik M, et al. Substrate binding and specificity of rhomboid intramembrane protease revealed by substrate-peptide complex structures. *EMBO J* 2014;33:2408–2421.
59. Jansson C, Debus RJ, Osiewacz HD, Gurevitz M, McIntosh L. Construction of an Obligate photoheterotrophic mutant of the cyanobacterium *Synechocystis* 6803: Inactivation of the *psbA* Gene Family. *Plant Physiol* 1987;85:1021–1025.
60. Lee T-C, Xiong W, Paddock T, Carrieri D, Chang I-F, et al. Engineered xylose utilization enhances bio-products productivity in the cyanobacterium *Synechocystis* sp. PCC 6803. *Metab Eng* 2015;30:179–189.
61. Bloye SA, Silman NJ, Mann NH, Carr NG. Bicarbonate Concentration by *Synechocystis* PCC6803: modulation of protein phosphorylation and inorganic carbon transport by glucose. *Plant Physiol* 1992;99:601–606.
62. Nieva M, Valiente EF. Inorganic carbon transport and fixation in cells of *Anabaena variabilis* adapted to mixotrophic conditions. *Plant Cell Physiol* 1996;37:1–7.
63. Koonin EV, Makarova KS, Rogozin IB, Davidovic L, Letellier M-C, et al. The rhomboids: a nearly ubiquitous family of intramembrane serine proteases that probably evolved by multiple ancient horizontal gene transfers. *Genome Biol* 2003;4:R19.
64. Mann NH, Novac N, Mullineaux CW, Newman J, Bailey S, et al. Involvement of an FtsH homologue in the assembly of functional photosystem I in the cyanobacterium *Synechocystis* sp. PCC 6803. *FEBS Lett* 2000;479:72–77.
65. Shao S, Cardona T, Nixon PJ. Early emergence of the FtsH proteases involved in photosystem II repair. *Photosynth* 2018;56:163–177.
66. Wang Y, Maegawa S, Akiyama Y, Ha Y. The role of L1 loop in the mechanism of rhomboid intramembrane protease GlpG. *J Mol Biol* 2007;374:1104–1113.
67. Baker RP, Young K, Feng L, Shi Y, Urban S. Enzymatic analysis of a rhomboid intramembrane protease implicates transmembrane helix 5 as the lateral substrate gate. *Proc Natl Acad Sci USA* 2007;104:8257–8262.
68. Adrain C, Cavadas M. The complex life of rhomboid pseudoproteases. *FEBS J* 2020;287:4261–4283.
69. Guichard A, Biehs B, Sturtevant MA, Wickline L, Chacko J, et al. Rhomboid and Star interact synergistically to promote EGFR/MAPK signaling during *Drosophila* wing vein development. *Development* 1999;126:2663–2676.
70. Han S-I, Nakakuki M, Nakagawa Y, Wang Y, Araki M, et al. Rhomboid protease RHBDL4/RHBDD1 cleaves SREBP-1c at endoplasmic reticulum monitoring and regulating fatty acids. *PNAS Nexus* 2023;2:pgad351.
71. Eysholdt-Derzsó E, Renziehausen T, Frings S, Frohn S, von Bongartz K, et al. Endoplasmic reticulum-bound ANAC013 factor is cleaved by RHOMBOLD-LIKE 2 during the initial response to hypoxia in *Arabidopsis thaliana*. *Proc Natl Acad Sci USA* 2023;120:e2221308120.
72. Bantu L, Chauhan S, Srikumar A, Hirakawa Y, Suzuki I, et al. A membrane-bound cAMP receptor protein, SyCRP1 mediates inorganic carbon response in *Synechocystis* sp. PCC 6803. *Biochim Biophys Acta Gene Regul Mech* 2022;1865:194803.
73. Kurkela J, Tyystjärvi T. Inorganic carbon sensing and signalling in cyanobacteria. *Physiologia Plantarum* 2024;176.
74. Haimovich-Dayan M, Kahlon S, Hihara Y, Hagemann M, Ogawa T, et al. Cross-talk between photomixotrophic growth and CO₂-concentrating mechanism in *Synechocystis* sp. strain PCC 6803. *Environ Microbiol* 2011;13:1767–1777.
75. Kanesaki Y, Yamamoto H, Paithoonrangsarid K, Shoumskaya M, Suzuki I, et al. Histidine kinases play important roles in the perception and signal transduction of hydrogen peroxide in the cyanobacterium, *Synechocystis* sp. PCC 6803. *Plant J* 2007;49:313–324.
76. McGrath JM, Long SP. Can the cyanobacterial carbon-concentrating mechanism increase photosynthesis in crop species? A theoretical analysis. *Plant Physiol* 2014;164:2247–2261.
77. Srivastava A, Shukla P. Tightening the screws on *psbA* in cyanobacteria. *Trends Genet* 2021;37:211–215.
78. Yi L, Liu B, Nixon PJ, Yu J, Chen F. Recent advances in understanding the structural and functional evolution of FtsH proteases. *Front Plant Sci* 2022;13:837528.
79. Yu F, Park S, Rodermeier SR. The *Arabidopsis* FtsH metalloprotease gene family: interchangeability of subunits in chloroplast oligomeric complexes. *Plant J* 2004;37:864–876.
80. Boehm M, Yu J, Krynicka V, Barker M, Tichy M, et al. Subunit organization of a *Synechocystis* hetero-oligomeric thylakoid FtsH complex involved in photosystem II repair. *Plant Cell* 2012;24:3669–3683.
81. Burnap RL, Hagemann M, Kaplan A. Regulation of CO₂ concentrating mechanism in cyanobacteria. *Life (Basel)* 2015;5:348–371.
82. Jiang Y-L, Wang X-P, Sun H, Han S-J, Li W-F, et al. Coordinating carbon and nitrogen metabolic signaling through the cyanobacterial global repressor NdhR. *Proc Natl Acad Sci USA* 2018;115:403–408.

Edited by: S. Gebhard and F. M. Commichau